Supplement: Vertical distribution of pollution trapped by wintertime surface inversions in Fairbanks, Alaska, during the ALPACA experiment

Jochen Stutz[1], Jonas Kuhn[1], Sol Cooperdock[1], Sarah Johnson[1], Fangzhou Guo[2,3], James H. Flynn[2], Meeta Cesler-Maloney[4], and William R. Simpson[4]

[1]Department of Atmospheric and Oceanic Science, University of California, Los Angeles, USA
[2]Department of Earth and Atmospheric Sciences, University of Houston, Houston, TX, USA
[3]Aerodyne Research Inc., Billerica, MA, USA
[4]University of Alaska, Fairbanks, AK, USA

Correspondence: Jochen Stutz (jochen@atmos.ucla.edu)

S1 DOAS Analysis

The analysis of the LP-DOAS spectra measured during ALPACA followed the principles outlined in Platt and Stutz (2008) and Stutz and Platt (1996). Trace gas concentrations from overlaying absorptions are retrieved using the combination of a linear and non-linear least squares fit of the sum of a scaled set of reference spectra (Stutz and Platt, 1996). Reference spectra were simulated using literature absorption cross sections convoluted with a slit function derived from a mercury emission line measured during ALPACA (Platt and Stutz, 2008). For NO_2, HCHO and O_3 we chose absorption cross section at 246 K, 253 K, and 253 K, respectively (Table S1). Since high spectral resolution, low-temperature cross-section are not available for HONO or SO_2,, we used room temperature cross sections (Table S1). Temperature variation in the SO_2 absorption cross section at lower spectral resolution are less than 10% (Bogumil et al., 2003). The temperature dependence of HONO absorptions is currently unknown, but it is likely in a similar range ($< \sim$10%) than NO_2. Temperature dependence of ozone and NO_2 were considered in the HONO, HCHO and SO_2 retrievals by including a reference spectrum describing the temperature dependence of NO_2 and O_3 (calculated as the orthogonal of reference spectra at two different temperatures) to reduce the error of these retrievals. Note that we did not consider temperature dependence of the O_3 and NO_2 cross sections when calculating the mixing ratios of these gases. We also included reference spectra for oxygen and oxygen collisional complexes. O_2 and O_2N_2 reference spectra were calculated for the light path length and O_2 and N_2 concentrations averaged over the campaign. The sources of these absorption cross sections are also listed in Table S1.

Concentrations of each trace gas were retrieved in specific wavelength windows to reduce systematic and random errors. These wavelength windows and the trace gases included in the fit are listed in Table S2. To take advantage of the larger differential absorption structures towards shorter wavelengths we performed an additional ozone measurement and retrieval for the lowest LP-DOAS path in a different wavelength window (282 nm – 307 nm). Because this wavelength range was measured about 5 minutes after our main UV range, we interpolated its O_3 data onto the time grid of the main range. Aside from the trace

Table S1. Absorption cross-section used in the DOAS analysis

O_3	253	Birk and Wagner (2018)
SO_2	298	Vandaele et al. (1994)
HCHO	253	Meller and Moortgat (2000)
NO_2	246	Voigt et al. (2002)
HONO	293	Stutz et al. (2000)
O_2	293	Rothman et al. (2010)
O_4	293	Hermans et al. (1999)
O_2N_2	293	Fally et al. (2000)

Table S2. Details on DOAS analysis

Trace gas	WL	Fitted Trace gases
O_3	292.1 – 320.5	O_3, SO_2, HCHO, NO_2
O_3 (lowest path)	282 – 307	O_3, SO_2, HCHO, NO_2, O_2, O_2N_2
SO_2	292.1-312.4	SO_2, O_3, HCHO, NO_2
NO_2	344.8 – 371.0	NO_2, HONO, HCHO, O_3, O_4
HCHO	311.1 – 332.0	HCHO, O_3, SO_2, NO_2
HONO	340.12 – 380.0	HONO, NO_2 , HCHO, O_3, O_4 (HCHO and NO_2 fixed to shorter WL fit results)

gas absorptions listed in Table S2 the first three orthogonal components of an singular value decomposition of all lamp spectra throughout the campaign was included in the fitting procedure, with the goal of capturing variations in the lamp spectra. In addition, a polynomial of degree 5 or 7 was included. All gas absorption spectra were shifted and squeezed with one set of common parameters to compensate for grating rotation errors and thermal shifts.

The results of our analysis for the entire experiment are shown in Figure S1. Data is displayed as mixing ratio at ambient temperature together with the measurement errors that were determined by each fitting procedure (Platt and Stutz, 2008; Stutz and Platt, 1997). Campaign average errors and errors at optimal instrument performance (best) are listed in Table S3 for the lowest path, 1, and the upper three paths, 2-4. The difference between the errors is due to the different path lengths. Detection limits are twice these errors.

S2 In-situ Observations

SO_2 was measured in-situ at 3 m aglL with a Thermo Scientific 43C instrument located in a stationary trailer parked next to the CTC building. Multi-point calibration of the SO_2 monitor was performed by overflowing the inlet with an EPA-certified mixed

Table S3. Campaign average and best measurement errors for path 1 and path 2-4

	Path 1		**Path 2-4**	
	best	average	best	average
	ppb	ppb	ppb	ppb
O_3	1.10	1.58	1.48	3.27
NO_2	0.08	0.15	0.13	0.33
SO_2	0.03	0.05	0.05	0.12
HCHO	0.13	0.28	0.24	0.58
HONO	0.02	0.04	0.03	0.08

standard (containing zero air, 5.190 ppm SO_2, and 508.4 ppm CO) diluted with zero air using an Environics 9100 calibration system and zero air.

Ozone and NOx were measured at the same location and height using a Thermo Scientific 49C and 42C instruments, respectively. A zero and multipoint calibration of the O_3 monitor was performed using the O_3 generator and calibration dilution system of the Environics 9100 system. The NOx monitor was calibrated using a similar method as SO_2 using a EPA certified NO standard of 50.12 ppm NO. NO_2 was produced using an excess of O_3 in the gas stream. All monitors were calibrated roughly every week. A second ozone monitor (Teledyne 400E) was deployed at Birch Hill at an altitude of 158 m above the valley floor. This monitor was calibrated through a ten-day intercomparison with the CTC monitor at the end of the field experiment.

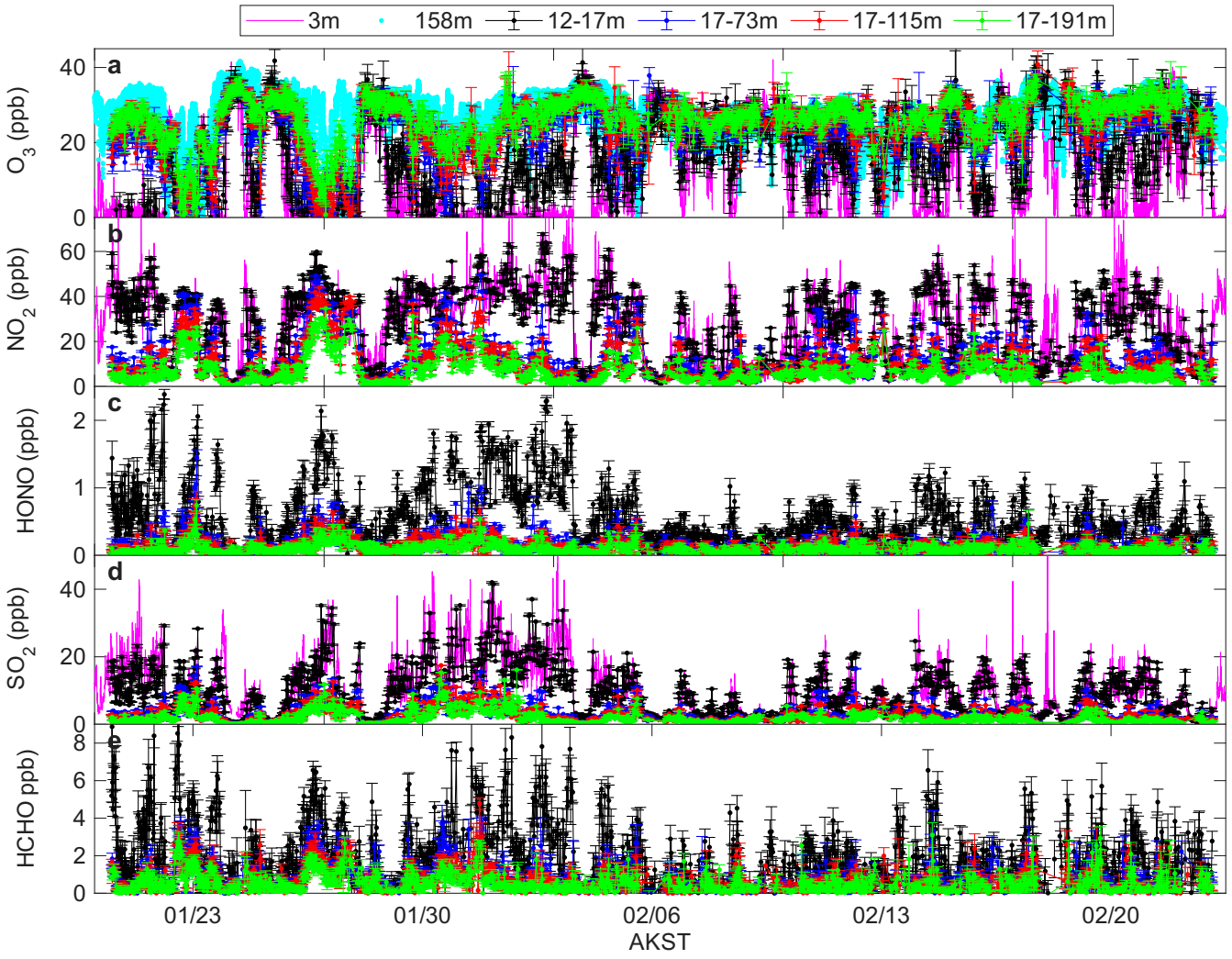

Figure S1. Campaign overview of the path-averaged LP-DOAS data along the four different lightpath using the same color coding as in Figure 1. Surface in-situ data is shown as a magenta line.

S3 Additional Figures

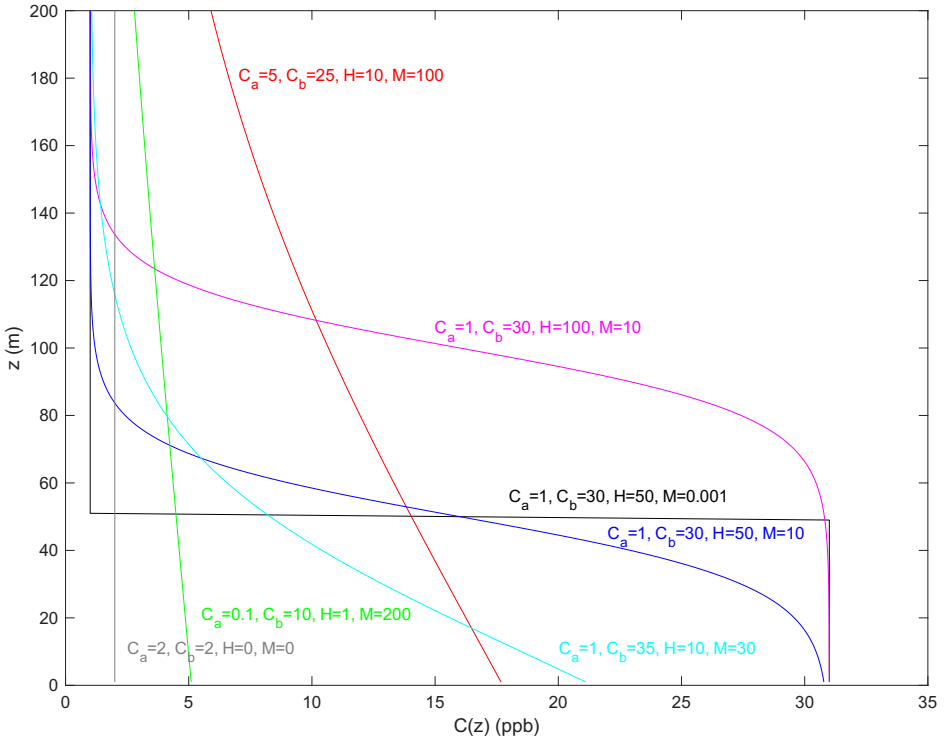

Figure S2. Shape of the sigmoid function (Eq. 1) used for the retrieval of vertical trace gas profiles from the LP-DOAS data. The curves show how various parameter combinations in Eq. 1 (Section 2.3) lead to different vertical profile shapes.

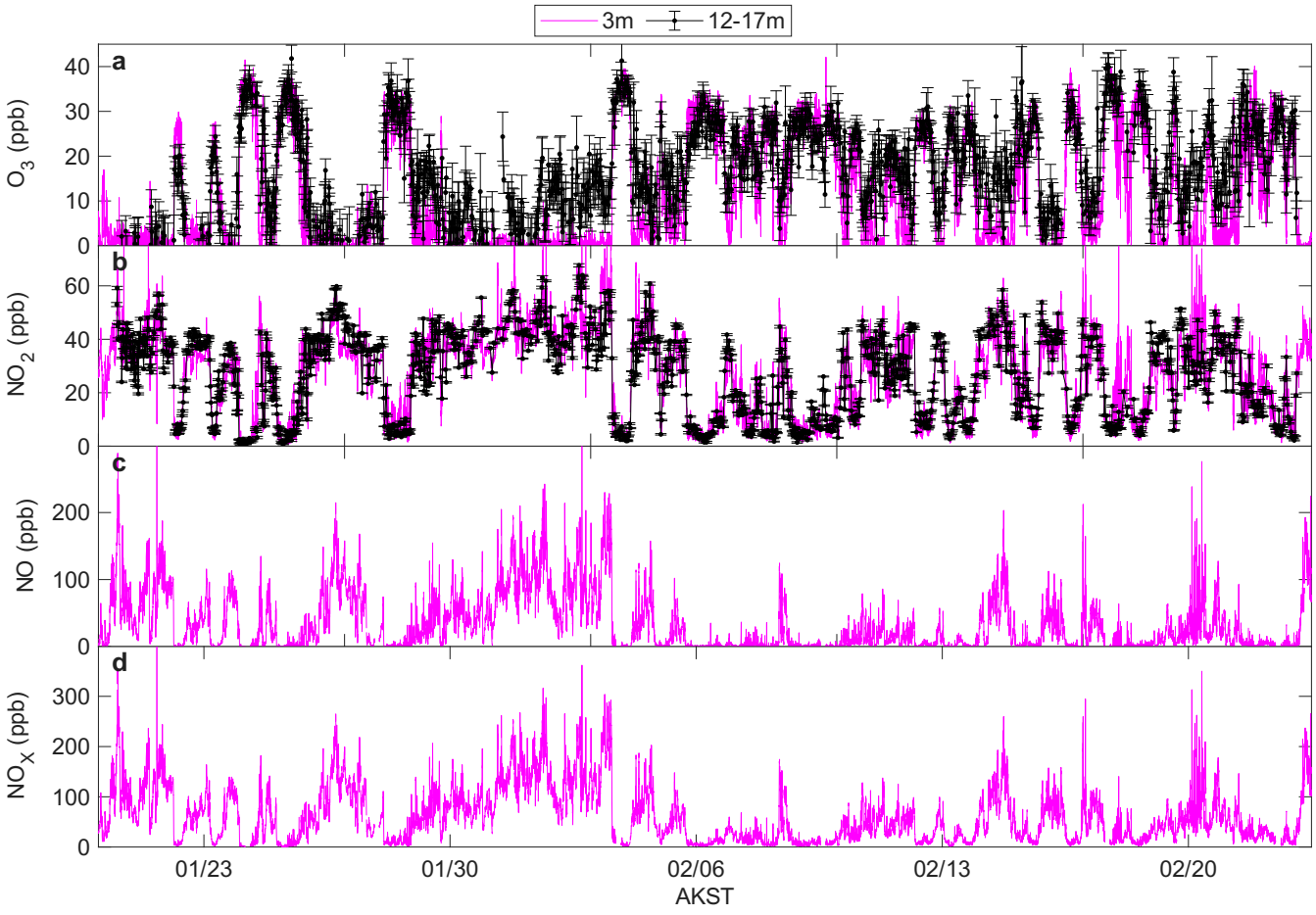

Figure S3. Campaign overview of PSL observations of (a) O_3, (b) NO_2, (c) NO, and (d) $NO_X = NO + NO_2$. Panels (a) and (b) compare LP-DOAS (12 - 17 m, black) and in-situ (3m, magenta) data. Only in-situ (3 m) data are shown in panels (c) and (d). Further explanation of this figure can be found in Section 3.1 in the main text.

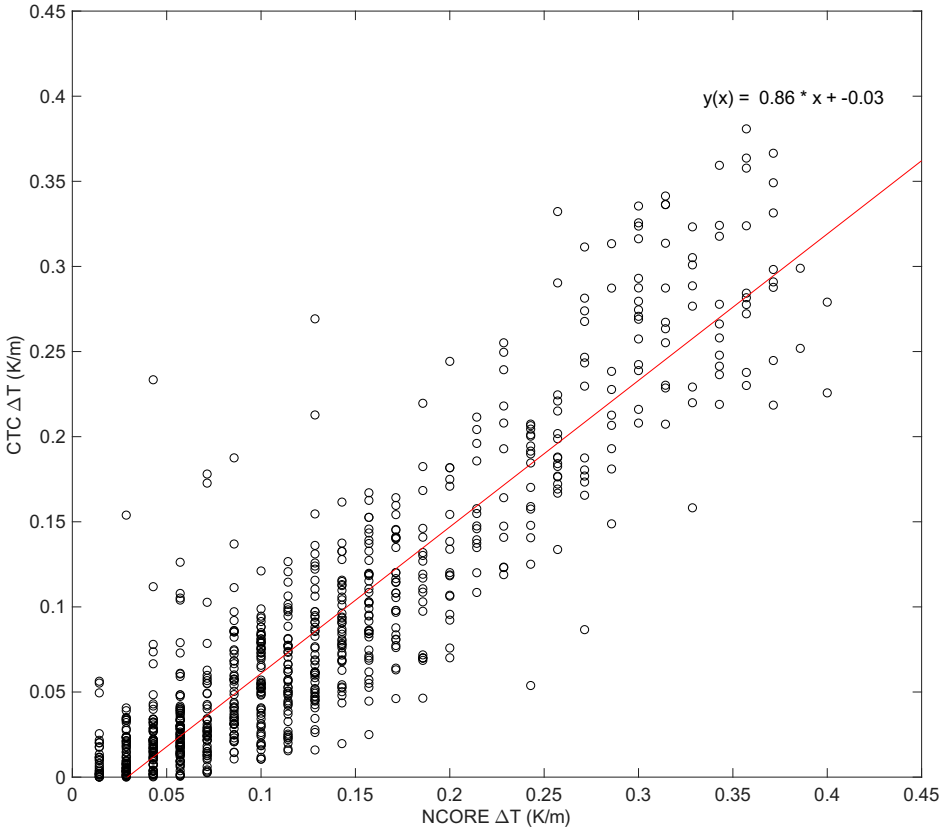

Figure S4. Comparison of CTC (11 - 3 m) and NCORE (10 - 3 m) temperature gradients (gradients below zero and above 0.4 $^{\circ}\mathrm{C}/\mathrm{m}$) were omitted from the fitting procedure to remove outliers). On average the CTC temperature gradients are about 14% smaller than the ones at NCORE.

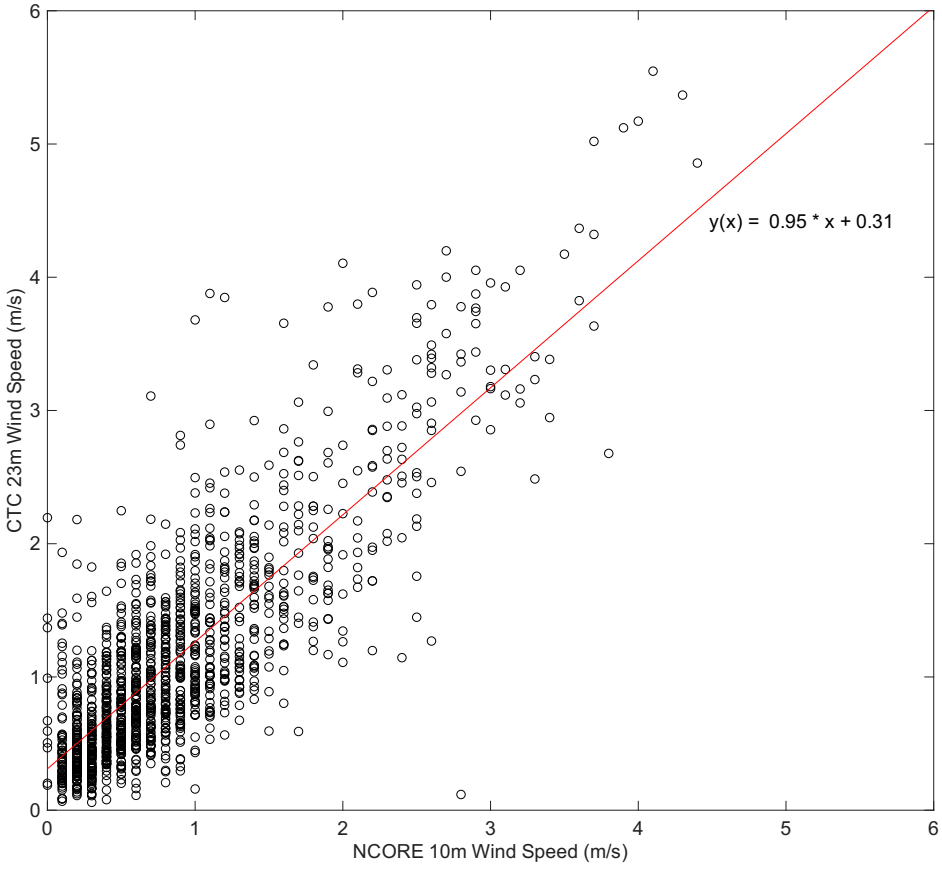

Figure S5. Comparison of CTC 23 m wind speed with NCORE 10 m wind speed. The two wind speeds agree surprisingly well with a slope of 0.95.

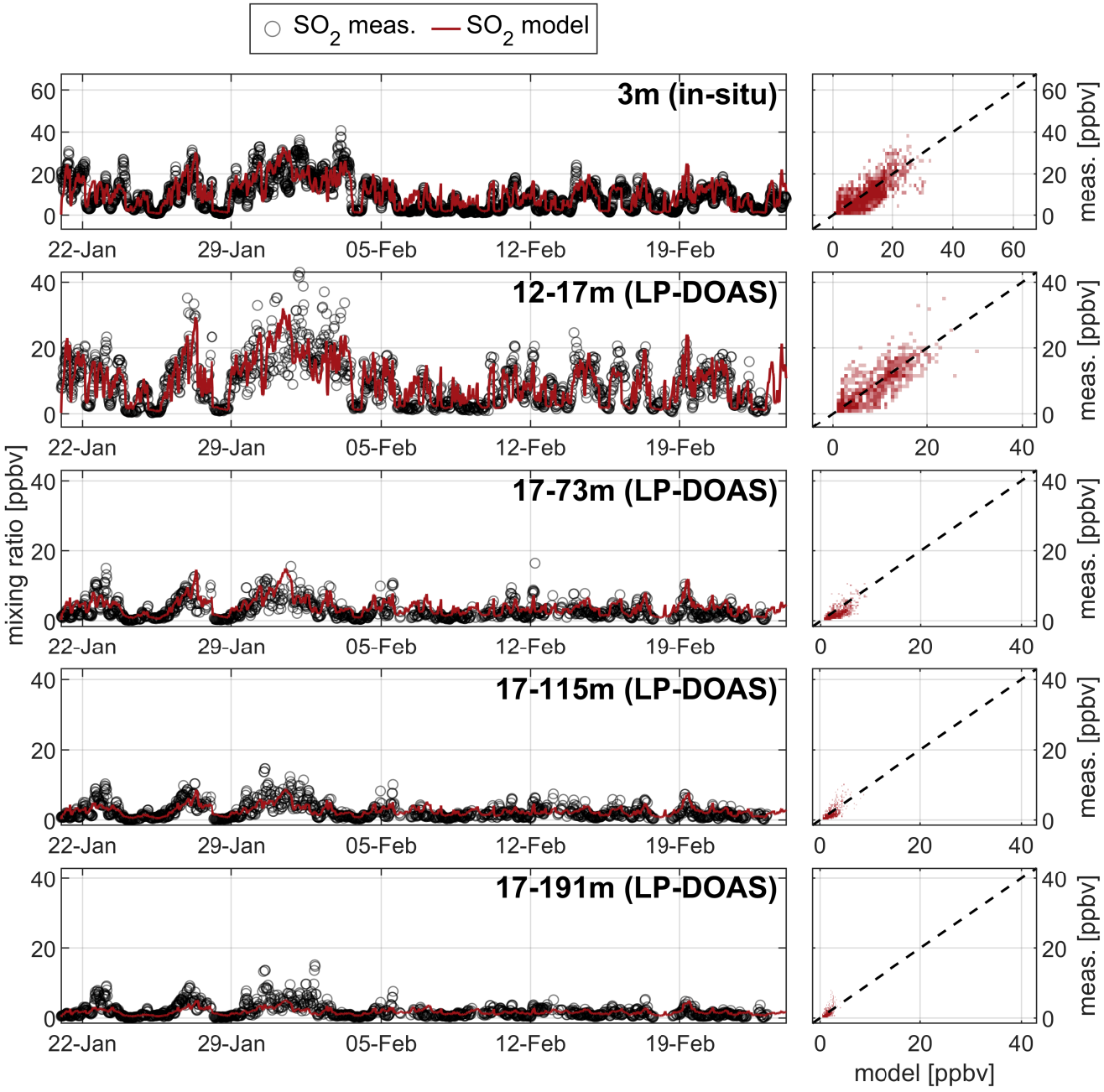

Figure S6. Comparison of in-situ and LP-DOAS observations of SO_2 with model output. The model data for the LP-DOAS comparison was averaged over the same height intervals as the respective light paths.

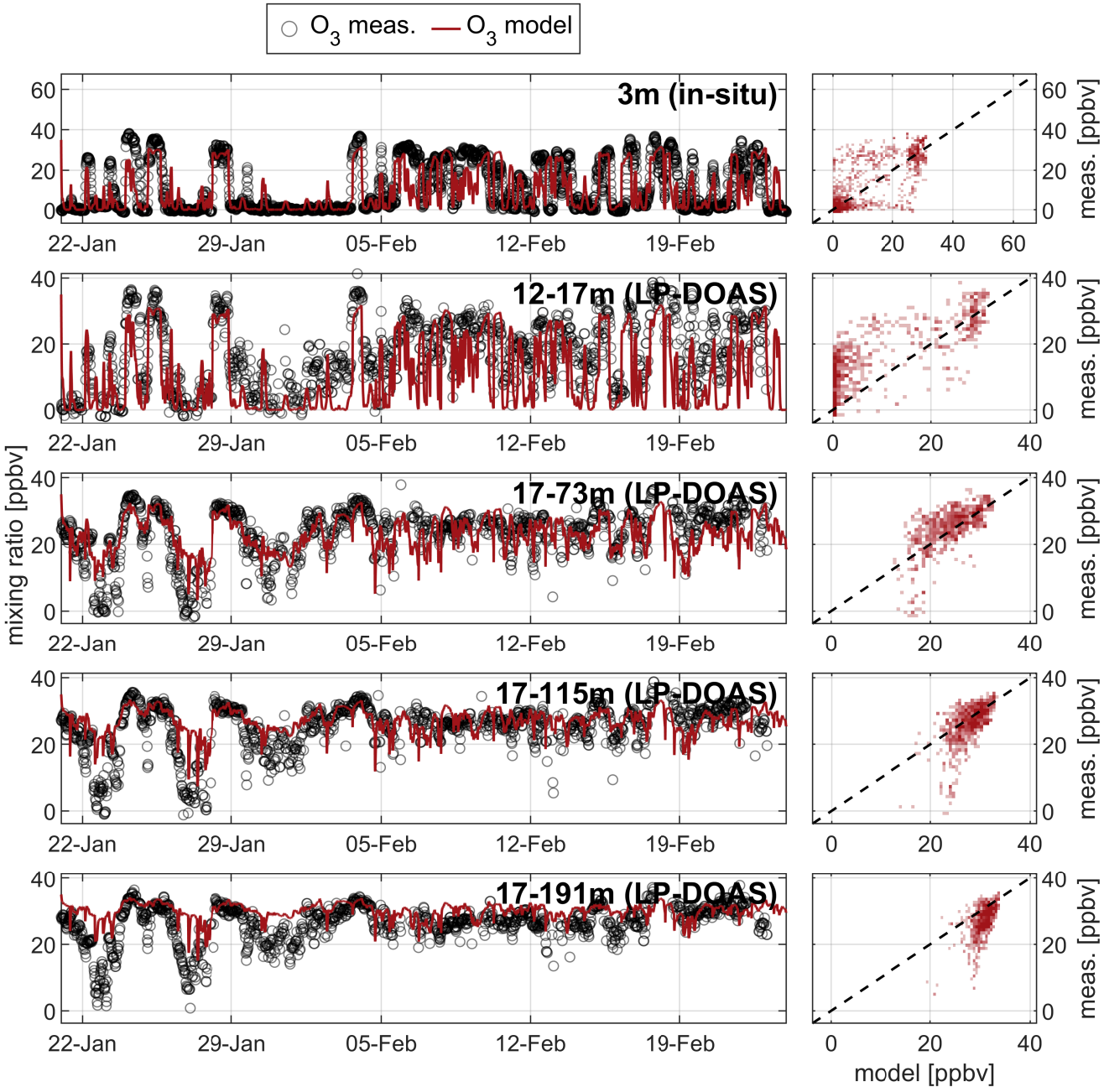

Figure S7. Comparison of in-situ and LP-DOAS observations of O3 with model output. The model data for the LP-DOAS comparison was averaged over the same height intervals as the respective light paths.

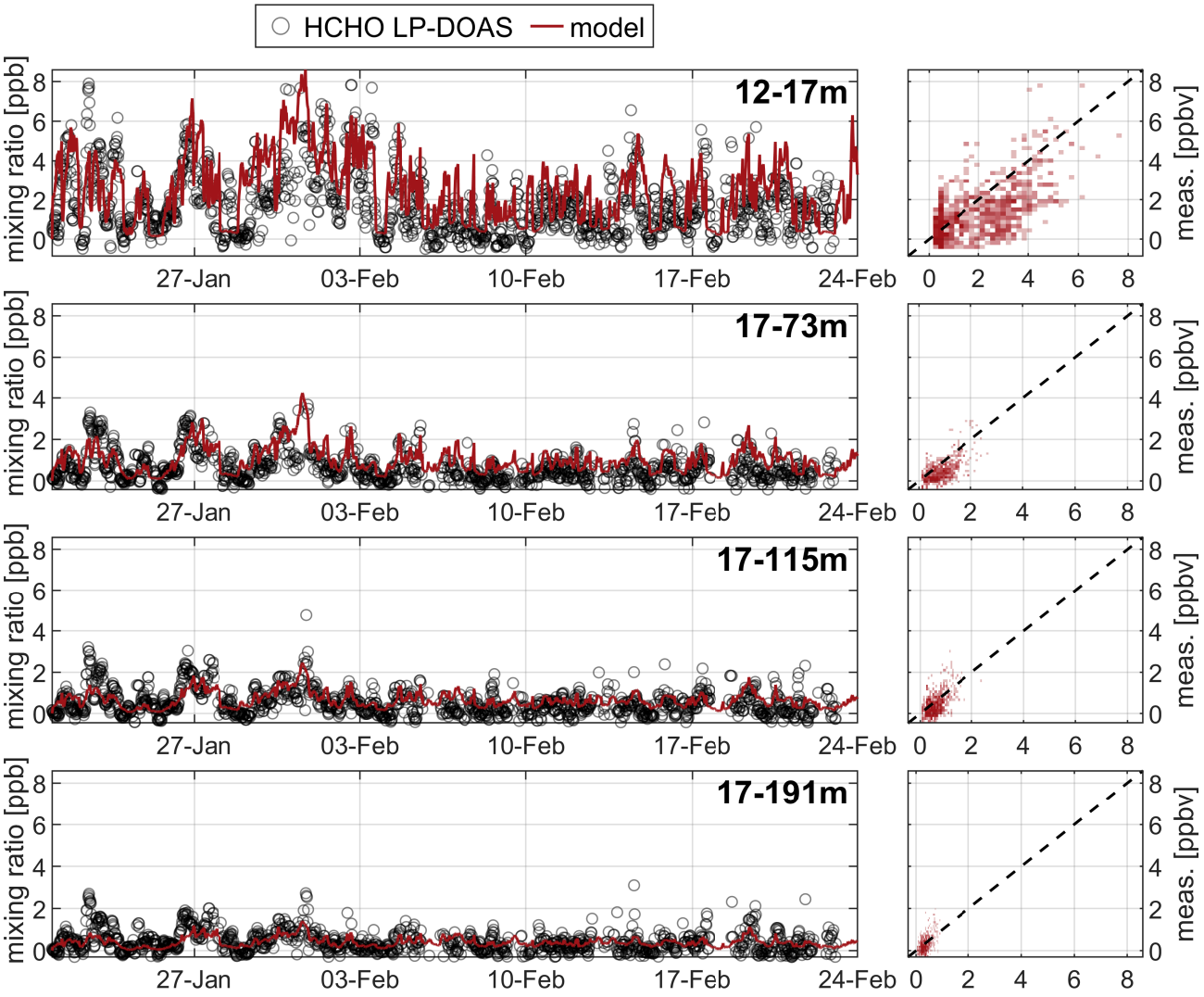

Figure S8. Comparison of LP-DOAS observations of HCHO with model output. The model data for the LP-DOAS comparison was averaged over the same height intervals as the respective light paths.

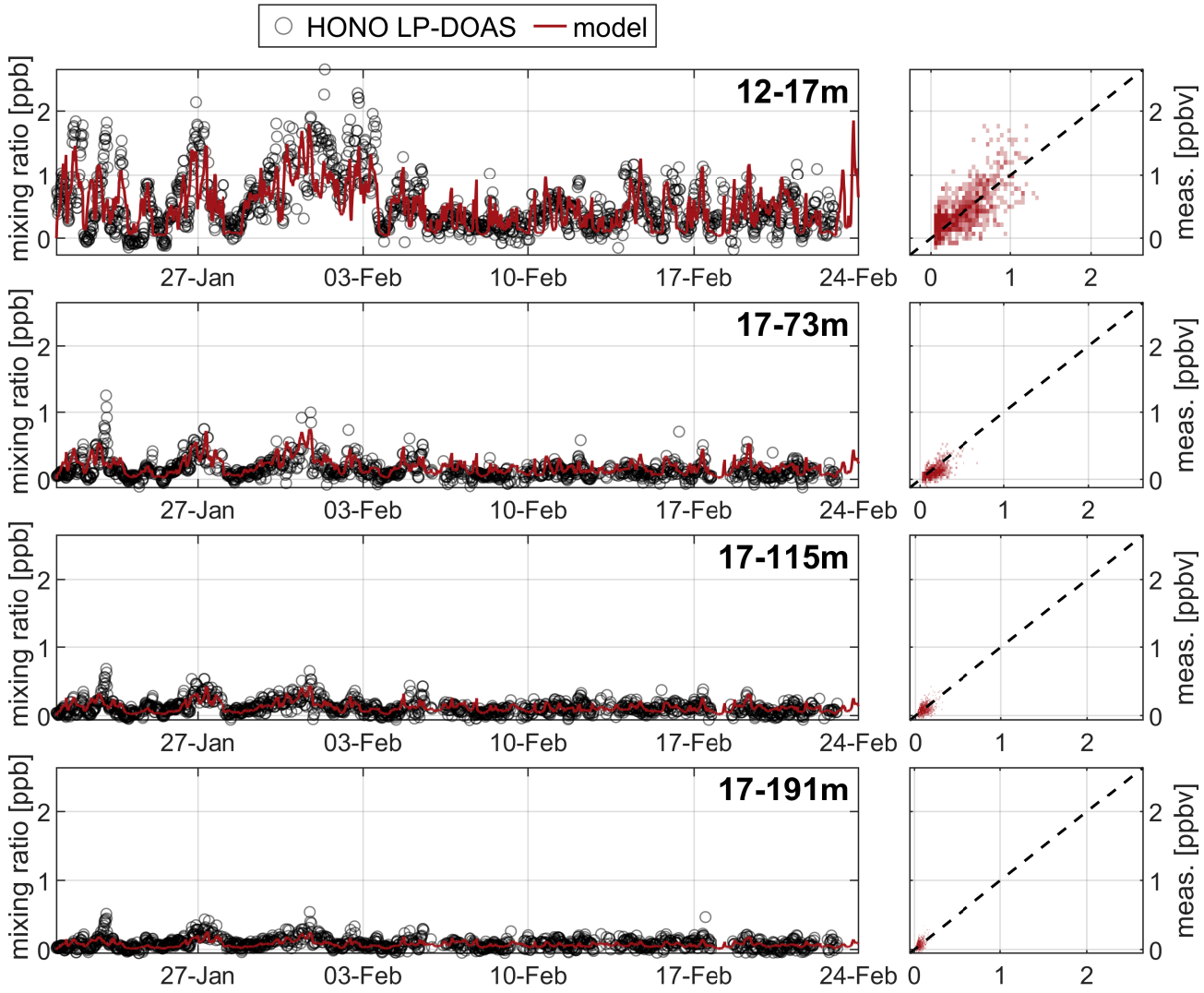

Figure S9. Comparison of LP-DOAS observations of HONO with model output. The model data for the LP-DOAS comparison was averaged over the same height intervals as the respective light paths.

References

Birk, M. and Wagner, G.: ESA SEOM-IAS – Measurement and ACS database O_3 UV region, https://doi.org/10.5281/zenodo.1485588, 2018.

Bogumil, K., Orphal, J., Homann, T., Voigt, S., Spietz, P., Fleischmann, O., Vogel, A., Hartmann, M., Kromminga, H., Bovensmann, H., Frerick, J., and Burrows, J.: Measurements of molecular absorption spectra with the SCIAMACHY pre-flight model: instrument characterization and reference data for atmospheric remote-sensing in the 230–2380 nm region, J. Photochem. Photobio. A: Chem, 157, 167–184, https://doi.org/10.1016/S1010-6030(03)00062-5, 2003.

Fally, S., Vandaele, A., Carleer, M., Hermans, C., Jenouvrier, A., Mérienne, M., Coquart, B., and Colin, R.: Fourier transform spectroscopy of the O_2 Herzberg Bands. III. Absorption cross sections of the collision-induced bands and of the Herzberg continuum., J. Molec. Spect., 204, 10–20, https://doi.org/10.1006/jmsp.2000.8204, 2000.

Hermans, C., Vandaele, A. C., Carleer, M., Fally, S., Colin, R., Jenouvrier, A., Coquart, B., and Mérienne, M. F.: Absorption cross-sections of atmospheric constituents: NO_2, O_2, and H_2O., Environ. Sci. Poll. Res., 6, 151, https://doi.org/10.1007/BF02987620, 1999.

Meller, R. and Moortgat, G. K.: Temperature dependence of the absorption cross sections of formaldehyde between 223 and 323 K in the wavelength range 225–375 nm, J Geophy. Res.: Atmos., 105, 7089–7101, https://doi.org/10.1029/1999JD901074, 2000.

Platt, U. and Stutz, J.: Differential Optical Absorption Spectroscopy, Springer Berlin Heidelberg, Berlin, Heidelberg, https://doi.org/10.1007/978-3-540-75776-4, 2008.

Rothman, L. S., Gordon, I. E., Barber, R. J., Dothe, H., Gamache, R. R., Goldman, A., Perevalov, V. I., Tashkun, S. A., and Tennyson, J.: HITEMP, the high-temperature molecular spectroscopic database, J. Quant. Spect. Rad. Trans., 111, 2139–2150, https://doi.org/10.1016/j.jqsrt.2010.05.001, 2010.

Stutz, J. and Platt, U.: Numerical analysis and estimation of the statistical error of differential optical absorption spectroscopy measurements with least-squares methods, Appl. Opt., 35, 6041–6053, https://doi.org/10.1364/AO.35.006041, 1996.

Stutz, J. and Platt, U.: Improving long-path differential optical absorption spectroscopy with a quartz-fiber mode mixer, Appl. Opt., 36, 1105–1115, https://doi.org/10.1364/AO.36.001105, 1997.

Stutz, J., Kim, E. S., Platt, U., Bruno, P., Perrino, C., and Febo, A.: UV-visible absorption cross sections of nitrous acid, J Geophy. Res.: Atmos., 105, 14 585–14 592, https://doi.org/10.1029/2000JD900003, 2000.

Vandaele, A., Simon, P., Guilmot, J., Carleer, M., and Colin, R.: SO_2 absorption cross section measurement in the UV using a Fourier transform spectrometer, J. Geophys. Res, 99, 25 599–25 605, https://doi.org/10.1029/94JD02187, 1994.

Voigt, S., Orphal, J., and Burrows, J.: The temperature and pressure dependence of the absorption cross-sections of NO_2 in the 250-800 nm region measured by Fourier-transform spectroscopy, Journal of Photochemistry and Photobiology A: Chemistry, 149, 1–7, https://doi.org/10.1016/S1010-6030(01)00650-5, 2002.